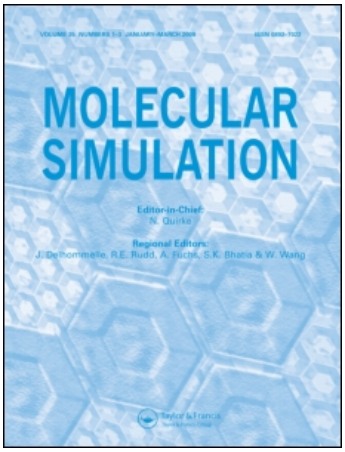

Molecular Simulation
Publication details, including instructions for authors and subscription information:
http://www.informaworld.com/smpp/title~content=t713644482

The importance of charge-quadrupole interactions for H_2 adsorption and diffusion in CuBTC

Jinchen Liu[a]; Rees B. Rankin[a]; J. Karl Johnson[ab]
[a] National Energy Technology Laboratory, Pittsburgh, USA [b] Department of Chemical and Petroleum Engineering, The University of Pittsburgh, Pittsburgh, USA

First published on: 21 September 2010

To cite this Article Liu, Jinchen , Rankin, Rees B. and Karl Johnson, J.(2009) 'The importance of charge-quadrupole interactions for H_2 adsorption and diffusion in CuBTC', Molecular Simulation, 35: 1, 60 — 69, First published on: 21 September 2010 (iFirst)
To link to this Article: DOI: 10.1080/08927020802398926
URL: http://dx.doi.org/10.1080/08927020802398926

Molecular Simulation
Vol. 35, Nos. 1–2, January–February 2009, 60–69

Taylor & Francis
Taylor & Francis Group

The importance of charge–quadrupole interactions for H_2 adsorption and diffusion in CuBTC

Jinchen Liu[ab], Rees B. Rankin[ab] and J. Karl Johnson[ab]*

[a]*National Energy Technology Laboratory, Pittsburgh, USA;* [b]*Department of Chemical and Petroleum Engineering, The University of Pittsburgh, Pittsburgh, USA*

(*Received 13 May 2008; final version received 9 August 2008*)

We have assessed the effects of charge–quadrupole interactions (CQIs) between the framework atoms of copper(II) benzene-1,3,5-tricarboxylate (CuBTC) and adsorbed H_2 molecules on equilibrium adsorption properties and self- and transport diffusivities. We have also compared charges computed from periodic density functional theory (DFT) on the fully periodic CuBTC structure with charges derived from DFT calculations on cluster models of CuBTC. Our results indicate that carboxylate group atom charges computed from plane wave periodic DFT with the Bader charge analysis formalism are not consistent with the charges computed from the ChelpG method from Gaussian-based DFT cluster calculations. The charges derived from Bader analysis seem to be too large. Adsorption isotherms computed from Monte Carlo simulations and diffusivities computed from molecular dynamics simulations indicate that CQIs have a substantial impact on equilibrium and transport properties of H_2 adsorbed in CuBTC at 77 K. Conversely, both adsorption isotherms and diffusivities were shown to be essentially unaffected by CQIs at 298 K.

Keywords: charge–quadrupole interactions; CuBTC; H_2 adsorption; H_2 diffusion; MOF

1. Introduction

Metal–organic framework materials (MOFs) have garnered a great deal of interest over the past several years as candidates for storage of gases such as methane and hydrogen and for separation of gas mixtures [1–15]. The advantages of MOFs when compared with many other nanoporous materials include their relatively low cost, high yield, adjustable pore size, shape and functionality, extremely high surface areas and the potential to be tailored for specific applications by changing the metals, ligands or linkers.

A key to design new MOFs for specific applications is the ability to accurately predict the adsorption and diffusion of fluids in MOFs from atomically detailed simulations. The adsorption isotherms computed from simulations are not always in agreement with the experimentally measured data, as noted in a recent review [16]. In some cases the discrepancy can be traced to problems with the experimental sample [16,17]. In other cases, a careful assessment of the potentials used in the simulations is needed. For example, Belof et al. [18] have shown that many-body polarisability effects can be very important for H_2 adsorbed in *soc*-MOF, which has a highly charged framework, while polarisability is not important for H_2 in IRMOF-1. Many of the simulations of H_2 adsorption in various MOF have ignored framework-H_2 charge–quadrupole interactions (CQIs), while obtaining a reasonably good agreement with experiments [19,20]. Other studies ignoring framework-H_2 CQIs have noted that predicted adsorption isotherms underpredict the experimental data [16,17,21]. Walton et al. [22] calculated adsorption isotherms for CO_2 in IRMOF-1, IRMOF-3 and MOF-177. They found that the inclusion of fluid–fluid quadrupole terms was critical for obtaining the good agreement with experiments. However, they ignored framework-CO_2 CQIs that are known to have a large impact on the adsorption of CO_2 in MOFs, especially below pressures of about 20 bar [23].

Given the lack of uniformity in accounting for framework-fluid CQIs, there is a need to critically assess the impact of CQIs on adsorption and diffusion. In this study, we have chosen to focus on a single MOF that has been extensively studied, both experimentally and theoretically, namely copper(II) benzene-1,3,5-tricarboxylate (CuBTC), also known as HKUST-1. This material was first synthesised in 1999 by Chui et al. [24] who published its structure based on X-ray diffraction measurements. Later on, Peterson et al. [25] published a slightly different structure for this same material based on neutron diffraction data.

In this paper, we investigate the effects of CQIs on H_2 adsorption and diffusion in CuBTC at 77 and 298 K. We begin our study by using periodic density functional theory (DFT) to characterise the two experimentally proposed structures. We next investigate the atomic charges in CuBTC. Atomic framework charges have previously been computed for CuBTC using a cluster model to represent the full periodic structure [26]. This is by far the most

*Corresponding author. Email: karlj@pitt.edu

ISSN 0892-7022 print/ISSN 1029-0435 online

DOI: 10.1080/08927020802398926
http://www.informaworld.com

common method used [16]. In this work, we use periodic DFT along with the Bader charge decomposition method [27] to estimate charges on the CuBTC framework atoms and compare our calculated values with our own cluster calculations and with previously published atomic charges [26]. We use framework charges from the literature and from our own calculations to assess the impact of CQIs on adsorption and diffusion of H_2 in CuBTC. The adsorption isotherms are computed from grand canonical Monte Carlo (GCMC) and both the self- and transport diffusivities are computed as a function of loading from equilibrium molecular dynamics.

2. Simulation techniques and calculation details

2.1 Models

We used a rigid structure to model CuBTC. The atomic coordinates of CuBTC were obtained from X-ray scattering experiments [24]; these coordinates included residual solvent molecules, which we have excluded. The interaction potential of a H_2 molecule with the CuBTC framework was calculated as a summation over all pair-wise interactions with the solid framework atoms, as given by

$$u_i = \sum_{j=1}^{N_f} \left(\phi_{ij} + u_{q_j\Theta}\right), \tag{1}$$

where ϕ_{ij} and $u_{q_j\Theta}$ are the van der Waals and CQIs terms for H_2 molecule i interacting with the atom j in the CuBTC framework, respectively. We employed the universal force field [28] for the framework atoms to represent the van der Waals part of the fluid-framework potentials, modelled by Lennard-Jones potentials. We have used two methods to account for the H_2-framework CQIs. For the first method, a point quadrupole moment on the H_2 molecule was used. The CQI term between a charged solid atom and the H_2 molecules is calculated by [29]

$$u_{q_j\Theta}(r, \phi_{ij}) = \frac{1}{8\pi\varepsilon_0}\frac{q_j\Theta_{H_2}(3\cos^2(\phi_{ij}) - 1)}{r_{ij}^3}. \tag{2}$$

Here, r_{ij} is the distance between atom j in the framework and the centre of mass of hydrogen molecule i, q_j is the charge on framework atom j (in units of Coulomb, C), Θ_{H_2} is the quadrupole moment of the hydrogen molecule, $\Theta_{H_2} = 2.1 \times 10^{-40}\,\mathrm{C\,m^2}$, ϕ_{ij} is the angle between the hydrogen molecule symmetry axis and the line connecting it with the framework atom and ε_0 is the vacuum permittivity. The summation of the CQIs was performed over 8 ($2 \times 2 \times 2$) unit cells of CuBTC in our simulations. We have verified that summation over 8 unit cells is converged.

The second method for accounting for CQIs used three point charges to represent the quadrupole moment of H_2. The H—H bond length was set to 0.74 Å, with a charge on each H atom of $+0.468e$, and a charge on the centre of mass of H_2 of $-0.936e$, as used previously [30]. The CQI was calculated by summation of the charge–charge interactions between each framework atom and each charge site of the H_2 molecule. These charge–charge interactions were pre-tabulated by a direct calculation of the atomic charge–charge interactions using 515 unit cells following the method developed by Skoulidas and Sholl [21].

In all cases, we used the Buch potential [31] to model the H_2–H_2 interactions ($\sigma = 2.96$ Å, $\varepsilon/k = 34.2$ K); the fluid-framework Lennard-Jones potentials were computed from Lorentz–Berthelot combining rules. The Lennard-Jones potentials were truncated at 17 Å without applying long-range corrections in the adsorption simulations. Note that we have not included an explicit fluid–fluid quadrupole term in our simulations, as discussed in Section 3.2. The diffusion calculations used a cut-off radius of 13 Å along with long-range corrections assuming a uniform density of framework atoms beyond the cut-off radius [32]. We have verified that the difference in the cut-offs with long-range corrections gives results that are indistinguishable from each other. This same method was used previously for simulating H_2 diffusion in a different MOF [33].

2.2 Simulation techniques

We used the conventional GCMC [34,35] simulation technique to compute adsorption isotherms. We started simulations at the lowest pressures from an empty MOF matrix and then successively increased the fugacity in each simulation. Each subsequent simulation was started from the final configuration of the previous run. Each simulation consisted of a total of 1×10^7 trial configurations; the first half of the configurations in each simulation was discarded for equilibration. A configuration is defined as an attempted translation, rotation, creation or deletion of a H_2 molecule. The probability of attempting a molecule creation or deletion was set to 0.3. An equation of state for hydrogen [36] was used to obtain the relationship between the bulk pressure and fugacity. We have converted the total adsorption obtained from simulation to excess adsorption to compare with the experiments. The details of the conversion calculations can be found in the literature [17].

We have employed equilibrium molecular dynamics simulations to compute the self- and corrected diffusivities for H_2 in CuBTC. We have performed 20 independent MD simulations at each loading, with simulation lengths of 2–3 ns after equilibrations of approximately 20 ps. We have calculated the transport diffusivity from

$$D_t(c) = D_0(c) \times \left(\frac{\partial \ln(f)}{\partial \ln(c)}\right)_T, \tag{3}$$

where $D_t(c)$ is the transport diffusivity ($\mathrm{cm^2/s}$), $D_0(c)$ is the corrected diffusivity ($\mathrm{cm^2/s}$), f is the fugacity of the

adsorbed fluid (in equilibrium with the bulk), c is the concentration of the adsorbate in the MOF and $(\partial \ln(f)/\partial \ln(c))_T$ is the thermodynamic correction factor that can be calculated from adsorption isotherms obtained from GCMC simulations. We have used a virial-type equation [37] to fit the adsorption isotherms, from which the thermodynamic correction factors were computed.

We used the Feynman–Hibbs effective (FH) potential [38,39] to represent the quantum effects for H_2 adsorption and diffusion in CuBTC at 77 K, following our previous work [17,33]. We ignored the quantum effects at room temperature since the quantum effects were found to be small at 298 K [17].

2.3 DFT calculation details

We have performed DFT calculations to quantitatively characterise the atomic structure of CuBTC. As a crystalline material, the ideal structure of CuBTC possesses a 624 atom unit cell with certain elements of symmetry. This unit cell can be mathematically reduced to a 156 atom primitive cell. The reduction of the simple unit cell to the primitive cell affords a significant enhancement in the computational feasibility for DFT calculations with CuBTC.

In order to characterise the CuBTC atomic structure, we have performed fully periodic plane-wave DFT calculations with the Vienna *ab initio* simulation package (VASP) [40,41]. In our calculations, we employed the PW-91 generalised gradient approximation (GGA) functional supplied in VASP. We have performed these GGA calculations using both the ultrasoft pseudopotential (USPP) [42,43] and the projector-augmented wave (PAW) [44,45] methods to account for inner core electrons. We have expanded the plane-wave basis sets in our calculations up to a cut-off energy of 400 eV for USPP calculations and 430 eV for PAW. The atomic coordinates of the CuBTC structure were optimised using the standard conjugate gradient algorithm in the VASP package until forces on all atoms were less than 0.04 eV/Å. For all results presented, the Monkhorst–Pack [46] scheme for k-point spatial sampling was used with grids of at least $3 \times 3 \times 3$ k-points. Atomic charges on the framework atoms were computed from our periodic DFT calculations using the Bader charge decomposition method [27].

We have also performed cluster-based DFT calculations on representative clusters of CuBTC to calculate atomic charges. These representative cluster fragment moieties of CuBTC were derived from the fully relaxed bulk atomic structures obtained from the periodic calculations. The clusters extracted from the periodic structures possess artificial dangling bonds. We have accounted for this effect by saturating these bonds with CH_3 groups or H atoms as appropriate. We performed the cluster DFT calculations using the Gaussian03 software suite [47]. The cluster calculations used the B3LYP/6-311++G(d,p) basis set. The ChelpG method was used to perform the charge partitioning of the electrostatic potential obtained from the cluster DFT calculations. The ChelpG method is generally accepted as the most reasonable and accurate method to derive representative atomic charges for use in model potentials [26,48].

3. Results and discussion

3.1 DFT calculations – CuBTC bulk structure and charges

In our fully periodic DFT calculations, we have constructed the 156 atom primitive cells corresponding to the experimentally reported structural unit cells of CuBTC from the work of Chui et al. [24] and Peterson et al. [25]. In our calculations, we began by geometrically optimising the full atomic structure of the primitive cell by minimising the forces on the atoms. We then performed calculations allowing a further optimisation of the cell shape and volume with accompanying optimisation of the atomic coordinates. The DFT calculations reveal that the optimised relaxed structures from both the experimental studies have very similar energies. The optimised CuBTC structure from the work of Chui is 0.035 eV/primitive cell higher in energy than the structure from the work of Peterson et al., using the PAW approach. This corresponds to an energy difference of 0.14 eV/unit cell or 0.001 eV/atom between the two structures. The results from USPP calculations are very similar, giving an energy difference of 0.055 eV/primitive cell.

The optimised lattice constant of CuBTC from our fully periodic DFT calculations was 26.39 Å for the structure of Chui et al. and 26.42 Å for the structure of Peterson et al. The calculations allowing the relaxation of cell shape did not produce significant deviations away from orthogonal cell vectors; the largest changes observed were of the order of 0.1–0.2° for both of the structures calculated. The lattice constants calculated are in good agreement with those reported from the experimental data. The lattice constant for the optimised structure of Chui et al. is within +0.2% of the experimental value (26.34 Å) and the corresponding value for the optimised structure of Peterson et al. is within +0.5% of the experimental value (26.31 Å). Another metric that allows a direct comparison of the DFT calculated optimised structure with the experimentally measured structure is the root mean square (RMS) displacement. An RMS calculation between the initial (derived from experimental data) coordinates of the CuBTC structure and the final (DFT-optimised) coordinates reveals the quantitative net geometric difference between the structures. The RMS values obtained for the CuBTC structures were 0.007 Å/atom for the structure of Chui et al. and 0.007 Å/atom for the structure of Peterson et al. The RMS value between the two fully relaxed DFT calculated structures is less than 0.01 Å/atom. The most significant deviations away from the experimental

structure positions as calculated by RMS correspond to the Cu and H atoms; some of these atoms deviate from the experimental structure position by up to 0.012 Å. Note that our calculations indicate that the two experimental structures do not relax to the same final structure. We conclude that the two structures are local minima. Indeed, there could be many similar structures separated by slight energetic differences with barriers between inter-conversion. The impact of slight differences in the crystal structure on simulated adsorption and diffusion properties has been shown to be very small [17,33].

We have calculated atomic point charges corresponding to the framework atoms of CuBTC using the fully periodic structures optimised via DFT calculations mentioned above. We have employed two distinct methods to determine these charges. The first method used was the Bader charge decomposition method [27] for VASP. The second method used was to construct fragment moieties of CuBTC derived from the DFT fully periodic bulk structure. We then calculated the atomic charges corresponding to these representative CuBTC framework structures using the ChelpG electronic partitioning scheme via DFT B3LYP/6-311++G(d,p) in the Gaussian03 software package. The structures used for the cluster DFT calculations are presented in Figure 1. We have used two different cluster sizes in our calculations, both of which are smaller than the cluster used by Yang and Zhong in their calculations [26]. Charges computed from non-periodic clusters must be renormalised in order to produce a charge neutral unit cell for the periodic structure. We renormalised the charges according to

$$q_i' = q_i - \sum_{i=1}^{N} x_i q_i, \tag{4}$$

where q_i' is the renormalised charge for species i, q_i is the charge computed from the cluster calculation, x_i is the fraction of species i having charge q_i in the fully periodic material and N is the number of distinct species. The results of these atomic charge calculations are summarised in Table 1, along with charges from the work of Yang and Zhong [26]. Note that the 30 atom cluster does not contain a C3 atom (see Figure 1). We therefore define the charge on C3 to be zero in this cluster. Yang and Zhong [26] used a slightly different basis set and a different fragment representation for the CuBTC framework. We find reasonably good agreement between the charges computed from the three cluster methods. However, results from the Bader charge calculations for the C1 and O1 atoms are inconsistent with the ChelpG charges from Gaussian calculation. In particular, the O atoms each gain approximately 0.4 extra electrons while the C1 atom loses 0.8 extra electrons. We show in Section 3.2 that these charges give rise to adsorption isotherms that are not in qualitative agreement with experiments. We therefore believe that the C1 and O1 charges are not physically realistic, although the other atoms have charges in relatively good agreement with the cluster model. The origin of this discrepancy is probably an artefact of the Bader charge partitioning method rather than being due to something inherent in the periodic DFT calculations.

3.2 *Effects of CQIs on H_2 adsorption*

We ignored the quadrupole–quadrupole interactions between H_2 molecules in our simulations because the Buch potential already includes these terms in the effective potential parameters. Adding the fluid–fluid quadrupole term in addition to the effective Lennard-Jones potential can make the H_2–H_2 interactions artificially too attractive [21]. To illustrate this point, we have calculated the bulk equation of state for H_2 at 77 K from GCMC simulations using the classical Buch potential, the FH effective Buch potential and the Darkrim–Levesque

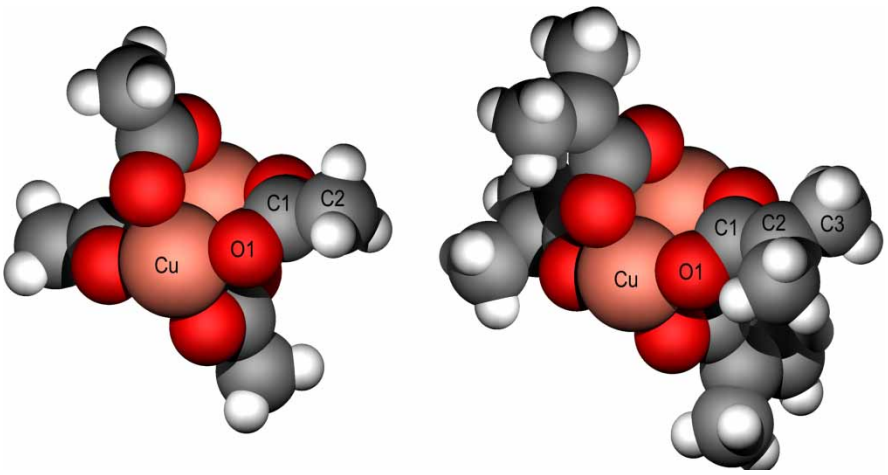

Figure 1. CuBTC fragment moieties derived from fully periodic DFT calculation used in ChelpG charge parameterisation using B3LYP calculations. At left, the 30 atom cluster, at right, the 50 atom cluster.

Table 1. Atomic partial charges as computed by DFT methods in this work and from Yang and Zhong [26].

Atomic species	Yang and Zhong [26]	ChelpG charges, this work		Bader charges, this work
		30 atom cluster	50 atom cluster	
Cu	1.098	1.105	1.082	1.01
O1	−0.665	−0.659	−0.725	−1.07
C1	0.778	0.937	0.824	1.50
C2	−0.092	−0.320	−0.061	0.06
C3	−0.014	0	−0.004	−0.05
H	0.109	0.150	0.153	0.11

model [30] with FH corrections. The calculated isotherms using different potentials are shown in Figure 2, along with experimental data from the literature [49]. The equation of state for H_2 is accurately reproduced by the FH-effective Buch potential [17], as can be seen in Figure 2. The FH effective Darkrim–Levesque potential slightly overestimates the density at a given pressure. The Darkrim–Levesque potential has Lennard-Jones parameters ($\sigma = 2.958$ Å, $\varepsilon/k = 36.7$ K) similar to those of the Buch potential ($\sigma = 2.96$ Å, $\varepsilon/k = 34.2$ K). The Buch potential has been shown to accurately reproduce the fluid properties of H_2 over a very wide range of temperatures and densities [50,51]. Hence, inclusion of the fluid–fluid quadrupole terms makes the Darkrim–Levesque potential artificially too attractive. We have used the FH correction truncated at the quadratic ($\hbar^2$) term because it has been shown to adequately represent the quantum effects at conditions relevant to this work [17,52,53]. Moreover, inclusion of the quartic ($\hbar^4$) term overcorrects for quantum effects [53], giving worse agreement with experiments and accurate path integral calculations than the second order approach.

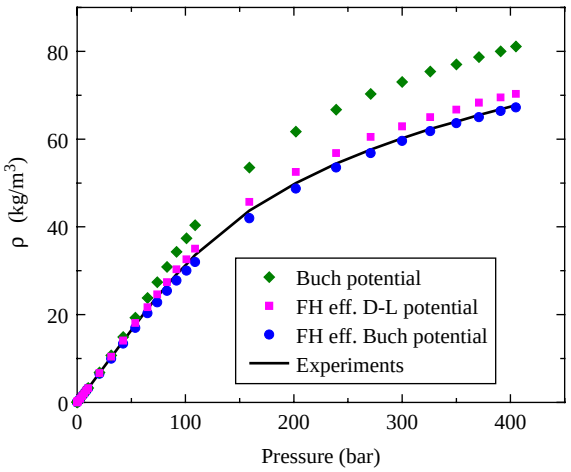

Figure 2. Equation of state for bulk H_2 at 77 K. The experimental data [49] are plotted as the solid line; the simulation results from the FH effective Darkrim–Levesque potential, Buch potential and FH effective Buch potential are represented by squares, diamonds and circles, respectively.

We have compared H_2 adsorption isotherms using both the point quadrupole and the point charge methods for calculating the CQIs. The isotherms agree with each other within the statistical uncertainty of the simulations over the entire range of pressures, as can be seen in Figure 3. The point quadrupole method is easy to implement and

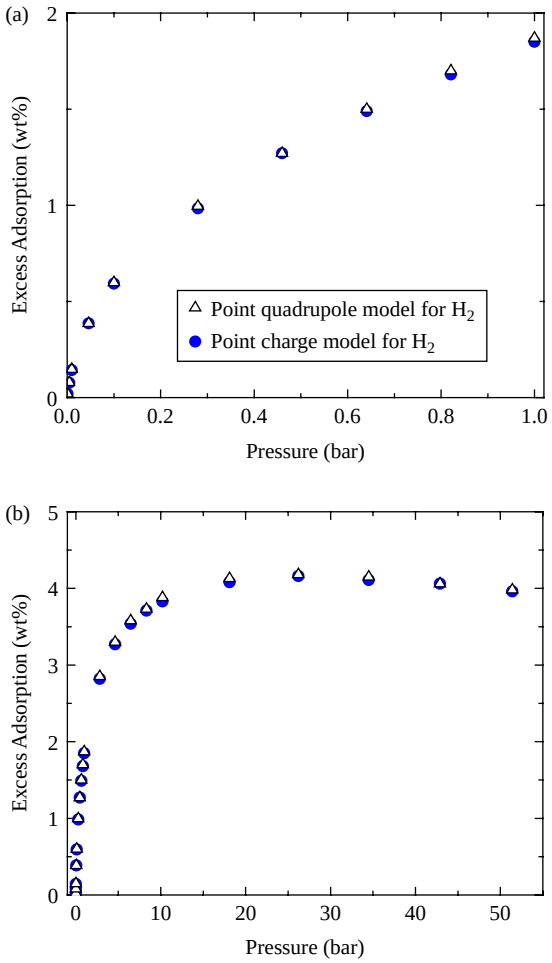

Figure 3. Comparison of H_2 adsorption isotherms in CuBTC at 77 K using two different charge–quadrupole models. (a) $P = 0$–1 bar (b) $P = 0$–50 bar. The simulation results from the point quadrupole and point charge models are represented by open triangles and filled circles, respectively.

computationally efficient, but less accurate for interactions at short distances. From this point forward, we will only present results calculated from the point charge model for the H_2 quadrupole.

We have used the charges on CuBTC framework atoms from Yang and Zhong [11,26], from our renormalised results of 50 atom cluster and from the Bader analysis in this work to calculate the H_2 adsorption isotherms at 77 K. We accounted for quantum effects by using the FH effective potential in these simulations. Isotherms computed using the charge schemes from Yang and Zhong and from our cluster calculations (not shown) are very similar, with our charge scheme giving about 0.1 wt% higher adsorption for $P > 1$ bar. We have compared simulation results with experiments and with the simulations without CQIs; this comparison is shown in Figure 4. Simulations using the charges from Bader analysis dramatically overestimate the amount adsorbed. There is a significant amount of adsorption at a pressure of 10^{-3} bar from simulations with the Bader charges, whereas the experiments and the other simulations show negligible adsorption for H_2 at these conditions. At this pressure, H_2 molecules mainly adsorb near the carboxyl groups in CuBTC due to very strong CQIs; these strong CQIs are caused by the unrealistically high atomic charges on carbon and oxygen atoms in the carboxyl groups (see Table 1). These results indicate that the charges from Bader analysis are incorrect.

Using the charges from Yang and Zhong [26] increases H_2 adsorption by about 12–17% at low pressure ($P \leq 1$ bar) and 10% at higher pressure region ($P > 10$ bar) at 77 K when compared with the FH–Buch potential ignoring CQIs. In the low-pressure region ($P \leq 1$ bar), the results for the FH–Buch plus CQIs are in almost perfect agreement with the Buch potential without quantum corrections [see Figure 4(a)]. Hence, inclusion of CQIs fortuitously cancels the quantum effects *at these conditions*. However, at pressures higher than about 5 bar, the Buch potential without quantum corrections overpredicts the amount adsorbed when compared with the FH corrected Buch + CQI potential (see Figure 4(b)). Moreover, we would not expect this fortuitous cancellation of quantum and charge effects to necessarily extend to other MOF materials. At low pressures inclusion of CQI terms still underestimates experimental adsorption data by about 30%, as can be seen in Figure 4(a). The H_2 adsorption isotherm calculated with CQIs agrees well with experiments above about 10 bar. Overall, the inclusion of CQIs improves the agreement with experiments, suggesting that CQIs should be accounted for when simulating adsorption of gases in polar MOF materials (i.e. MOFs having strong local dipoles) or polar molecules in MOF materials. However, there is still a discrepancy at low pressures, where all our simulations with reasonable potentials underestimate the amount adsorbed relative to experiment.

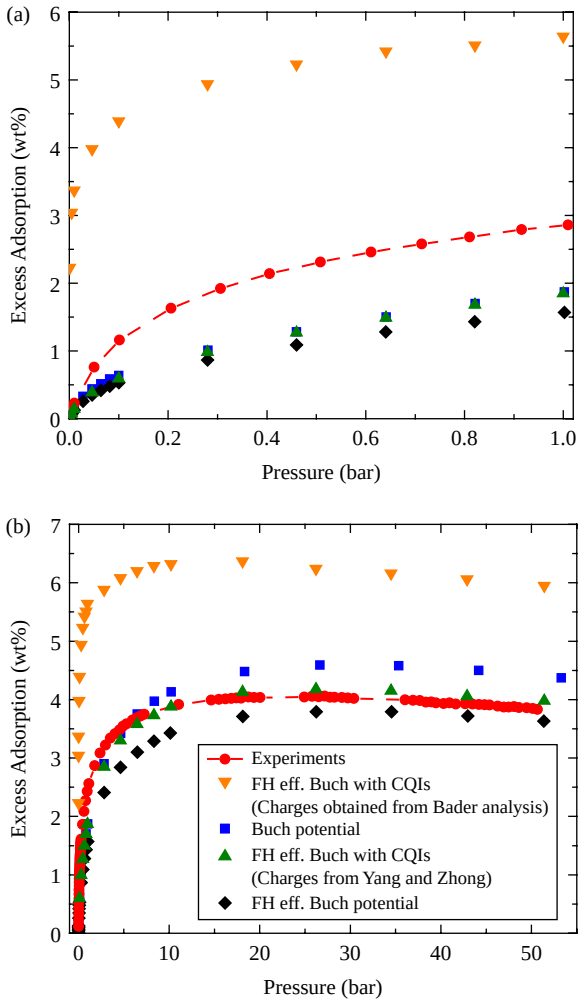

Figure 4. Comparison of simulated and experimental H_2 adsorption isotherms in CuBTC at 77 K. (a) $P = 0$–1 bar. (b) $P = 0$–50 bar. The experimental results [17] are represented by filled circles. The simulation results using classical Buch potential and FH effective potential are represented by squares and diamonds, respectively and are taken from our previous work [17]. The simulation results using FH effective potential with CQIs using charges from Yang and Zhong [26] and Bader analysis are represented by up triangles and down triangles, respectively.

In addition to the 77 K calculations, we have also calculated isotherms at 298 K using various potentials and have compared our calculations with the experimental data from Liu et al. [17] in Figure 5. As we previously observed for simulations at 77 K, using the charges from Bader analysis significantly overestimates the amount H_2 adsorbed. The amount adsorbed increases only 0.02 wt% at $P = 50$ bar using the charges from Yang and Zhong [26] when compared the results calculated ignoring CQIs. In this case, both simulations (with and without CQIs) agree well with the experimental data. CQIs are essentially negligible at 298 K. The reason for this is that the charge–quadrupole terms largely cancel at high temperature

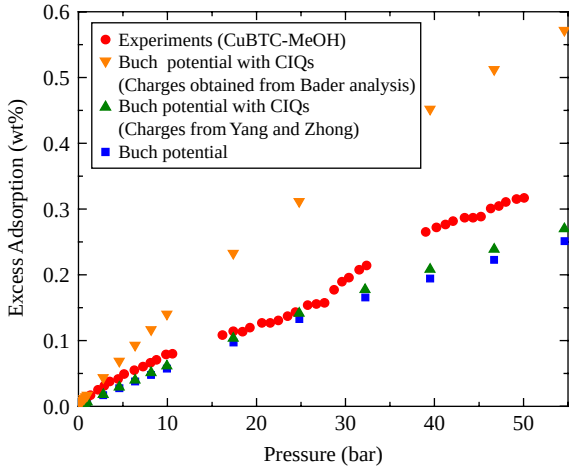

Figure 5. Comparison of simulated and experimental H_2 adsorption isotherms in CuBTC at 298 K. The experimental results [17] are represented by filled circles. The simulation results without CQIs, taken from [17], with CQIs for charges from Yang and Zhong [26] and CQIs with charges from Bader analysis are represented by squares, up triangles and down triangles, respectively.

because the adsorbate molecules behave as nearly free rotors. The CQI as given by Equation (2) is both positive and negative, depending on the orientation of the molecule. Therefore, the angle average of Equation (2), appropriate for free rotors, is a factor of 4 smaller than the most attractive orientation.

3.3 *Effects of CQIs on H_2 diffusion*

We have computed the self-diffusivities of H_2 in CuBTC at 77 K using three different potentials: the Buch potential, the FH-effective Buch potential and the FH-effective Buch potential with CQIs, using charges from Yang and Zhong [26]. The results are plotted in Figure 6. The self-diffusivities show the same trends and have similar numerical values for all the three potentials used. The self-diffusivity increases with increasing pressure (loading) in the low-pressure (loading) region, then decreases in the high-pressure (loading) region after reaching a maximum value. This qualitative behaviour was previously observed for CH_4 and Ar diffusion in a pure silica MFI-type zeolite, ITQ-3 [54]. The topology of CuBTC is similar to ITQ-3 in that both materials have large and small cages. In CuBTC, the small and large pores have diameters of 5 and 9 Å, respectively, and are connected by a window of about 4.5 Å in diameter [24]. In the low-pressure (loading) region, H_2 molecules mainly adsorb in the small pores and diffusion is limited by the energy barrier required to escape the small pores. At higher (intermediate) loadings H_2 begins to adsorb in the large pores on the surface of the linker. This results in a decrease in the energy barrier for

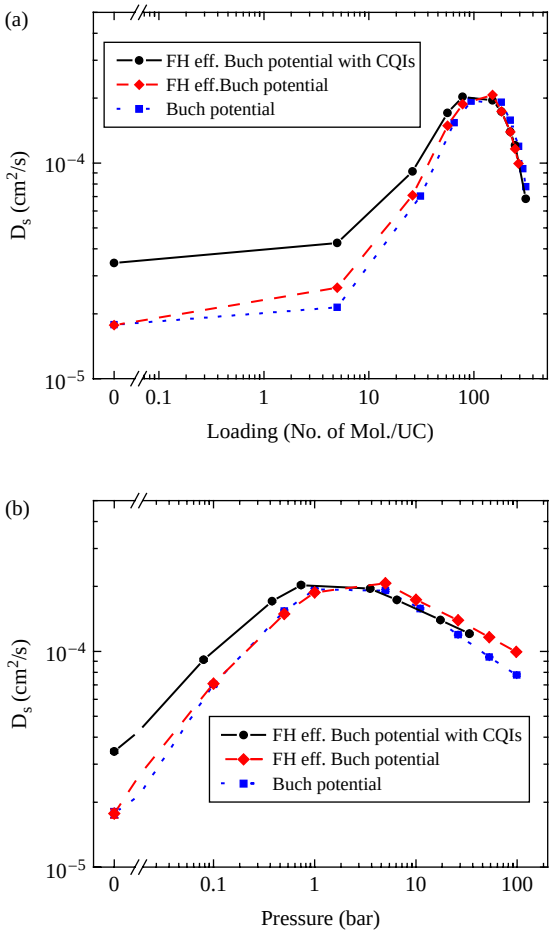

Figure 6. Simulated self-diffusivities of H_2 in CuBTC at 77 K (a) in terms of loading, (b) in terms of pressure. The simulation results with CQIs for charges from Yang and Zhong are represented by circles. The simulation results without CQIs using the Buch potential and FH effective Buch potential are represented by squares and diamonds, respectively. The lines are a guide to the eye.

diffusion out of the small pores and hence increases the diffusivity. At high loadings, the steric hindrance between the adsorbate molecules leads to a decrease in the self-diffusivity.

From Figure 6 we see that at low pressures, $P < 1$ bar, (less than 100 H_2 per unit cell), inclusion of CQIs increases self-diffusivities by about 20–80% when compared with the simulations ignoring CQIs. We have calculated the activation energies at zero loading for temperatures of 77, 100, 150 and 200 K. The activation energies were computed from the Arrhenius plot of the self-diffusivities. The calculated activation energies are 3.5 and 4.1 kJ/mol for the simulations with and without the CQIs, respectively. The observation of the H_2 diffusion trajectories at low loadings reveals that the rate controlling step is diffusion out of the small pores. The lower activation energy calculated with the inclusion of CQIs

compared with that without CQIs indicates that the CQIs decrease the energy barrier for a molecule going from the small pores to the large pores. This decrease in the energy barrier results in an increase in the self-diffusivity. The inclusion of the FH-effective term has negligible effects on self-diffusivities at low loadings compared with the classical Buch potential.

The self-diffusivities at high loadings are essentially identical when plotted as a function of loading (Figure 6(a)). This is a result of diffusivity being mainly controlled by adsorbate–adsorbate scattering above a loading of about 100 molecules per unit cell.

We have plotted the H_2 transport diffusivities at 77 K using the above three potentials in Figure 7. The H_2 transport diffusivities increase monotonically with increasing pressure, a result consistent with the studies for the diffusion of other gases in MOF materials [32,33].

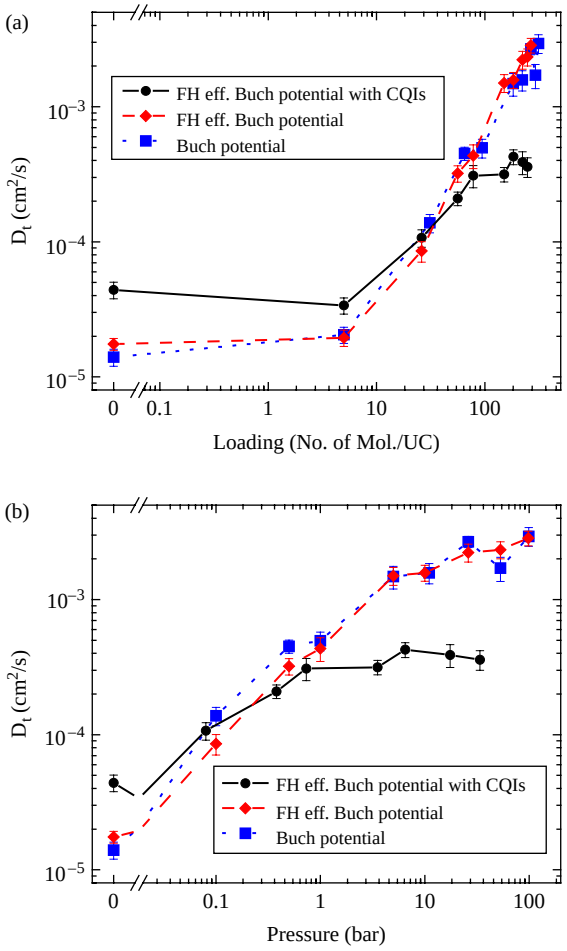

Figure 7. Simulated transport diffusivities of H_2 in CuBTC at 77 K (a) in terms of loading and (b) in terms of pressure. The simulation results with CQIs for charges from Yang and Zhong are represented by circles. The simulation results without CQIs using Buch potential and FH effective Buch potential are represented by squares and diamonds, respectively. The lines are a guide to the eye.

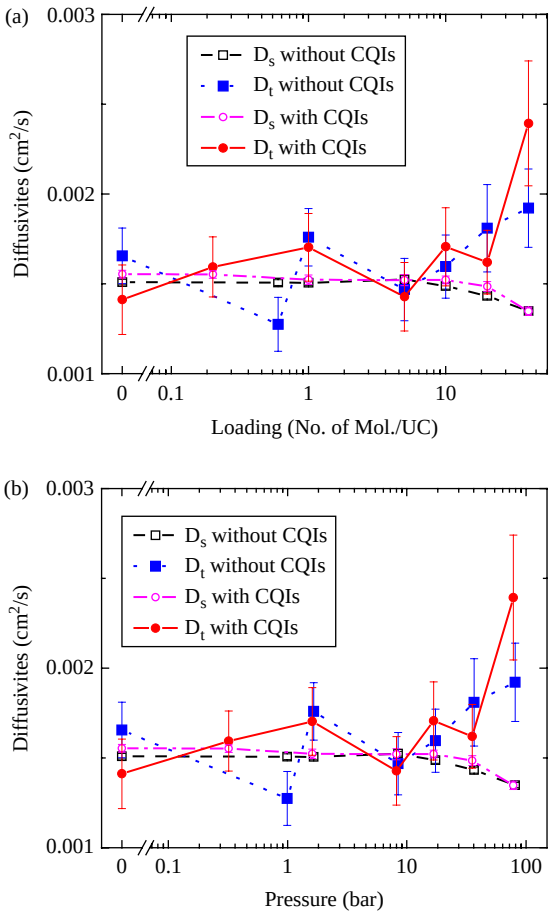

Figure 8. Simulated self- (open symbols) and transport (solid symbols) diffusivities of H_2 in CuBTC at 298 K (a) in terms of loading and (b) in terms of pressure. The simulation results without CQIs and with CQIs for charges from Yang and Zhong are represented by squares and circles, respectively. The lines are a guide to the eye.

The transport diffusivities calculated by including CQIs are larger (smaller) than those without CQIs at low (high) loadings.

We have plotted the self- and transport diffusivities at 298 K as calculated with and without CQIs in Figure 8. The diffusivities with and without CQIs are essentially identical within the statistical uncertainties in the data. Hence, charge–quadrupole terms do not have a significant effect on transport properties at room temperature. This observation is consistent with the adsorption isotherms at 298 K shown in Figure 4.

4. Conclusions

We have used DFT methods to compute structural and energetic properties of CuBTC. The energies of the DFT relaxed experimental structures from Chui et al. [24] and Peterson et al. [25] are within 0.14 eV/unit cell of each

other. Thus, these two structures are essentially energetically degenerate. We have also performed fully periodic as well as cluster-based DFT calculations to estimate the atomic partial charges in the CuBTC framework. The charges for the fully periodic structure were computed by the Bader charge analysis method, while the cluster models employed the ChelpG method. Our cluster-based ChelpG charges agree well with the values reported by Yang and Zhong [26]. However, the Bader analysis method was seen to significantly overestimate the charges on the COO group.

We have employed statistical mechanical simulation methods to investigate the effect of CQIs on adsorption and diffusion of H_2 in CuBTC. We have compared simulations using CuBTC charges from the literature and from Bader charge analysis from our calculations. Inclusion of charges from the literature increases the agreement between simulations and experiments for adsorption at 77 K, whereas the Bader charges result in much higher adsorption than observed experimentally. Hence, we conclude that Bader charges should be very carefully examined to determine if they are suitable for constructing interatomic potentials for use in statistical mechanical simulations. Inclusion of charges at 298 K had negligible effect on the adsorption isotherm.

Self- and transport diffusivities have been computed for H_2 in CuBTC, both with and without CQIs, at 77 and 298 K. As with adsorption isotherms, CQIs have a substantial impact on diffusion at 77 K but are negligible at 298 K. Hence, inclusion of adsorbate–adsorbent charge–quadrupole interactions may be important for computing the adsorption and diffusion of gases in MOF materials. We expect, for example, that CQIs would be very important for CO_2 adsorption and diffusion in MOFs, even at room temperature, because of the very large CO_2 quadrupole.

Acknowledgements

We thank Anant Kulkarni and Yang Wang for their helpful discussions. Funding for this work has been provided by the U.S. Department of Energy through the National Energy Technology Laboratory under grant No. 41817M203841817M2000.

References

[1] M. Eddaoudi, H. Li, and O.M. Yaghi, *Highly porous and stable metal–organic frameworks: structure design and sorption properties*, J. Amer. Chem. Soc. 122 (2000), pp. 1391–1397.

[2] Q.M. Wang, D.M. Shen, M. Bulow M.L. Lau, S. Deng, F.R. Fitch, N. Lemcoff, and O.J. Semanscin, *Metallo-organic molecular sieve for gas separation and purification*, Microporous Mesoporous Mater. 55 (2002), p. 217.

[3] R.Q. Snurr, J.T. Hupp, and S.T. Nguyen, *Prospects for nanoporous metal–organic materials in advanced separations processes*, AIChE J. 50 (2004), pp. 1090–1095.

[4] T. Düren and R.Q. Snurr, *Assessment of isoreticular metal–organic frameworks for adsorption separations: a molecular simulation study of methane/*n*-butane mixtures*, J. Phys. Chem. B 108 (2004), pp. 15703–15708.

[5] T. Düren, L. Sarkisov, O.M. Yaghi, et al., *Design of new materials for methane storage*, Langmuir 20 (2004), pp. 2683–2689.

[6] J.L.C. Rowsell and O.M. Yaghi, *Strategies for hydrogen storage in metal–organic frameworks*, Angew. Chem. Int. Ed. 44 (2005), pp. 4670–4679.

[7] A.R. Millward and O.M. Yaghi, *Metal–organic frameworks with exceptionally high capacity for storage of carbon dioxide at room temperature*, J. Amer. Chem. Soc. 127 (2005), pp. 17998–17999.

[8] J.L.C. Rowsell, E.C. Spencer, J. Eckert, et al., *Gas adsorption sites in a large-pore metal organic framework*, Science 309 (2005), pp. 1350–1354.

[9] A.G. Wong-Foy, A.J. Matzger, and O.M. Yaghi, *Exceptional H_2 saturation uptake in microporous metal–organic frameworks*, J. Amer. Chem. Soc. 128 (2006), pp. 3494–3495.

[10] L. Pan, D.H. Olson, L.R. Ciemnolonski, et al., *Separation of hydrocarbons with a microporous metal–organic framework*, Angew. Chem. Int. Ed. 45 (2006), pp. 616–619.

[11] Q. Yang and C. Zhong, *Electrostatic-field-induced enhancement of gas mixture separation in metal–organic frameworks: a computational study*, Chemphyschem. 7(7) (2006), pp. 1417–1421.

[12] Q. Yang, C. Xue, C. Zhong, et al., *Molecular simulation of separation of CO_2 from flue gases in Cu-BTC metal–organic framework*, AIChE J. 53(11) (2007), pp. 2832–2840.

[13] R. Babarao, Z. Hu, J. Jiang, et al., *Storage and separation of CO_2 and CH_4 in silicalite, C168 schwarzite, and IRMOF-1: a comparative study from Monte Carlo simulations*, Langmuir 23 (2007), pp. 659–666.

[14] S. Keskin and D.S. Sholl, *Screening metal–organic framework materials for membrane-based methane/carbon dioxide separations*, J. Phys. Chem. C 111 (2007), pp. 14055–14059.

[15] S. Wang, Q. Yang, and C. Zhong, *Adsorption and separation of binary mixtures in a metal–organic framework Cu-BTC: a computational study*, Sep. Purif. Technol. 60 (2008), pp. 30–35.

[16] S. Keskin, J. Liu, R.B. Rankin, et al., *Progress, opportunities, and challenges for applying atomically-detailed modeling to molecular adsorption and transport in metal–organic framework materials*, Ind. Eng. Chem. Res. (2008), DOI 10.1021/ie800666s.

[17] J.-C. Liu, J.T. Culp, S. Natesakhawat, B.C. Bockrath, B. Zande, S.G. Sankar, G. Garberoglio, and J. Karl Johnson, *Experimental and theoretical studies of gas adsorption in $Cu_3(BTC)_2$: an effective activation procedure*, J. Phys. Chem. C 111(26) (2007), pp. 9305–9313.

[18] J.L. Belof, A.C. Stern, M. Eddaoudi, et al., *On the mechanism of hydrogen storage in a metal–organic framework material*, J. Amer. Chem. Soc. 129(49) (2007), pp. 15202–15210.

[19] H. Frost, T. Duren, and Q. Snurr, *Effects of surface area, free volume, and heat of adsorption on hydrogen uptake in metal–organic frameworks*, J. Phys. Chem. B 110 (2006), pp. 9565–9570.

[20] H. Frost and R.Q. Snurr, *Design requirements for metal–organic frameworks as hydrogen storage materials*, J. Phys. Chem. C 111 (2007), pp. 18794–18803.

[21] G. Garberoglio, A.I. Skoulidas, and J.K. Johnson, *Adsorption of gases in metal organic materials: comparison of simulations and experiments*, J. Phys. Chem. B 109 (2005), pp. 13094–13103.

[22] K.S. Walton, A.R. Millward, D. Dubbeldam, et al., *Understanding inflections and steps in carbon dioxide adsorption isotherms in metal–organic frameworks*, J. Amer. Chem. Soc. 130(2) (2008), pp. 406–407.

[23] Q. Yang, C. Zhong, and J.-F. Chen, *Computational study of CO_2 storage in metal–organic frameworks*, J. Phys. Chem. C 112 (2008), pp. 1562–1569.

[24] S.S.Y. Chui, S.M.F. Lo, J.P. Charmant, et al., *A Chemically functionalizable nanoporous material $[Cu_3(TMA)_2(H_2O)_3]_n$*, Science 283(5405) (1999), pp. 1148–1150.

[25] V.K. Peterson, Y. Liu, C.M. Brown, and C.J. Kepert, *Neutron powder diffraction study of D_2 sorption in Cu_3(1,3,5-benzenetricarboxylate)$_2$*, J. Amer. Chem. Soc. 128(49) (2006), pp. 15578–15579.

[26] Q.-Y. Yang and C.-L. Zhong, *Molecular simulation of carbon dioxide/methane/hydrogen mixture adsorption in metal–organic frameworks*, J. Phys. Chem. B 110 (2006), pp. 17776–17783.

[27] G. Henkelman, A. Arnaldsson, and H. Jonsson, *A fast and robust algorithm for Bader decomposition of charge density*, Comput. Mater. Sci. 36 (2006), pp. 354–360.
[28] A.K. Rappe, C.J. Casewit, K.S. Colwell, W.A. Goddard, and W.M. Skiff, *Uff, a full periodic-table force-field for molecular mechanics and molecular-dynamics simulations*, J. Amer. Chem. Soc. 25 (1992), pp. 10024–10035.
[29] V.V. Simonyan, P. Diep, and J.K. Johnson, *Molecular simulation of hydrogen adsorption in charged single-walled carbon nanotubes*, J. Chem. Phys. 111 (1999), pp. 9778–9783.
[30] F. Darkrim and D. Levesque, *Monte Carlo simulations of hydrogen adsorption in single-walled carbon nanotubes*, J. Chem. Phys. 109 (1998), pp. 4981–4984.
[31] V. Buch, *Path-integral simulations of mixed para-D-2 and ortho-D-2 clusters – the orientational effects*, J. Chem. Phys. 100(10) (1994), pp. 7610–7629.
[32] A.I. Skoulidas and D.S. Sholl, *Self-diffusion and transport diffusion of light gases in metal–organic framework materials assessed using molecular dynamics simulations*, J. Phys. Chem. B 109 (2005), pp. 15760–15768.
[33] J.-C. Liu, J.Y. Lee, L. Pan, et al., *Adsorption and diffusion of hydrogen in a new metal–organic framework material: [Zn(bdc)(ted)$_{0.5}$]*, J. Phys. Chem. C 112 (2008), pp. 2911–2917.
[34] M.P. Allen and D.J. Tildesley, *Computer Simulation of Liquids*, Oxford University Press, New York, 1987.
[35] D. Frenkel and B. Smit, *Understanding Molecular Simulation: From Algorithms to Applications*, 2nd ed., Academic Press, San Diego, 2002.
[36] B.A. Younglove, *Thermophysical properties of fluids. I. Argon, ethylene,* para*hydrogen, nitrogen, nitrogen trifluoride, and oxygen*, J. Phys. Chem. Ref. Data Suppl. 11(1) (1982), pp. 1–354.
[37] L. Czepirski and J. Jagiello, *Virial-type thermal equation of gas–solid adsorption*, Chem. Eng. Sci. 44 (1989), pp. 797–801.
[38] R.P. Feynman, *Statistical Mechanics; A Set of Lectures*, W.A. Benjamin, Reading, MA, 1972.
[39] R.P. Feynman and A.R. Hibbs, *Quantum Mechanics and Path Integrals*, McGraw-Hill, New York, 1965.
[40] G. Kresse and J. Furthmuller, *Efficient iterative schemes for* ab initio *total-energy calculations using a plane-wave basis set*, Phys. Rev. B 54(16) (1996), pp. 11169–11186.
[41] G. Kresse and J. Hafner, Ab initio *molecular dynamics for liquids*, Phys. Rev. B 47 (1993), pp. 558–561.
[42] G. Kresse and J. Hafner, *Norm-conserving and ultrasoft pseudopotentials for first-row and transition elements*, J. Phys. Cond. Mat. 6 (1994), pp. 8245–8257.
[43] D. Vanderbilt, *Soft self-consistent pseudopotentials in a generalized eigenvalue formalism*, Phys. Rev. B 41(11) (1990), pp. 7892–7895.
[44] P.E. Blöchl, *Projector augmented-wave method*, Phys. Rev. B. 50(24) (1994), pp. 17953–17979.
[45] G. Kresse and D. Joubert, *From ultrasoft pseudopotentials to the projector augmented-wave method*, Phys. Rev. B, 59(3) (1999), pp. 1758–1775.
[46] H.J. Monkhorst and J.D. Pack, *Special points for Brillouin-zone integrations*, Phys. Rev. B 13(12) (1976), pp. 5188–5192.
[47] M.J. Frisch, G.W. Trucks, H.B. Schlegel, G.E. Scuseria, M.A. Robb, J.R. Cheesman, J.A. Montgomery Jr, T. Vreven, K.N. Kudin, J.C. Burant, et al., *Gaussian03*, Gaussian, Inc., Pittsburgh, 2003.
[48] H. Heinz and U.W. Suter, *Atomic charges for classical simulations of polar systems*, J. Phys. Chem. B 108(47) (2004), pp. 18341–18352.
[49] NIST. *NIST Standand Reference Database 69* (2005), Available at http://webbook.nist.gov
[50] Q. Wang and J.K. Johnson, *Phase equilibrium of quantum fluids from simulation: hydrogen and neon*, Fluid Phase Equilibria 132 (1997), pp. 93–116.
[51] Q. Wang, J.K. Johnson, and J.Q. Broughton, *Thermodynamic properties and phase equilibrium of fluid hydrogen from path integral simulations*, Mol. Phys. 89 (1996), pp. 1105–1119.
[52] L.M. Sese, *Study of the Feynman–Hibbs effective potential against the path-integral formalism for Monte-Carlo simulations of quantum many-body Lennard-Jones systems*, Mol. Phys. 81(6) (1994), pp. 1297–1312.
[53] L.M. Sese, *Feynman–Hibbs potentials and path-integrals for quantum Lennard-Jones systems – theory and Monte-Carlo simulations*, Mol. Phys. 85(5) (1995), pp. 931–947.
[54] A.I. Skoulidas and D.S. Sholl, *Molecular dynamics simulations of self-diffusivities, corrected diffusivities, and transport diffusivities of light gases in four silica zeolites to assess influences of pore shape and connectivity*, J. Phys. Chem. A 107 (2003), pp. 10132–10141.